Journal of Crystal Growth 600 (2022) 126910

Contents lists available at ScienceDirect

Journal of Crystal Growth

journal homepage: www.elsevier.com/locate/jcrysgro

The optimal threading dislocation density of AlN template for micrometer-thick $Al_{0.63}Ga_{0.37}N$ heteroepitaxy

Chia-Yen Huang [a,*], Sylvia Hagedorn [b], Sebastian Walde [b], Chia-Lung Tsai [c], Yi-Keng Fu [c], Markus Weyers [b]

[a] Department of Photonics, College of Electrical and Computer Engineering, National Yang Ming Chiao Tung University, Hsinchu 30010, Taiwan
[b] Ferdinand-Braun-Institut (FBH), Gustav-Kirchhoff-Strasse 4, 12489 Berlin, Germany
[c] Electronic and Optoelectronic System Research Laboratories, Industrial Technology Research Institute, 195, Sec.4, Chung Hsing Rd., Hsinchu, Taiwan

A R T I C L E I N F O

Communicated by Hilde Hardtdegen

Keywords:
A1. Line defects
A1. Stresses
A3. Metalorganic vapor phase epitaxy
B1. Nitrides
B2. Semiconducting ternary compounds
B3. Light emitting diodes

A B S T R A C T

Growth of Si-doped AlN and of $Al_{0.63}Ga_{0.37}N$ on high quality AlN templates grown by HVPE has been investigated. The strain state of Si-doped AlN is thickness-dependent due to the surface-mediated dislocation tilt which induces a tensile strain component. At very low dislocation density in the AlN buffer strain relaxation in micrometer-thick $Al_{0.63}Ga_{0.37}N$ layers is dominated by generation of additional dislocations. As a result, the final threading dislocation density and the surface roughness increase significantly. For a 1.6 μm $Al_{0.63}Ga_{0.37}N$ on 3.4 μm Si-doped AlN bi-layer structure, the optimal threading dislocation density (TDD) of the AlN:Si buffer is estimated to be 7×10^8 cm^{-2}, where the low TDD can be still transferred from the buffer to the thick AlGaN heterostructure without generation of many new dislocations.

1. Introduction

For III-nitride optoelectronics, threading dislocations (TDs) in the active region are non-radiative recombination centers. TDs with a screw component contribute to carrier leakage through devices [1,2]. Although the internal quantum efficiency (IQE) of InGaN-based emitters is less sensitive to threading dislocation density (TDD) in comparison with devices in other III-V materials system [3,4], GaN templates with a reduced TDD have brought about improvement in device performance. For example, InGaN-based light-emitting diodes (LEDs) were initially grown on flat sapphire with low-temperature (LT) GaN and AlN buffer layers [5,6]. In the 2000s, patterned sapphire substrate (PSS) technology gradually took over in commercial application. GaN-on-PSS templates not only promote the light extraction efficiency of LED chips, but also further reduce the TDD by the grain coalescence process [7]. In the 2010s, some groups promoted GaN-on-GaN violet LEDs for high-end luminaires [8]. The IQE of GaN-on-GaN LED was estimated to be >90 % due to the ultra-low TDD from the bulk GaN substrates.

AlGaN-based deep-UV (DUV) LEDs followed a similar path. Lowering the TDD of AlN templates to improve the IQE of DUV LEDs was and is an active research topic. Unfortunately, the metal–organic chemical vapor epitaxy (MOVPE) of AlN-on-sapphire is more challenging than that of GaN due to the high reactivity of Al atoms and their low mobility on the growing surface. Although new MOVPE growth techniques were developed for AlN templates [9–11], the TDD of AlN was still much higher (>2×10^9 cm^{-2}) than that of conventional GaN templates. Epitaxial lateral overgrowth also effectively lowers the TDD of AlN [12,13], but the poor Al adatom mobility resulted in a much higher coalescence thickness. Although the TDD of bulk AlN substrate was demonstrated to be lower than 1×10^7 cm^{-2} [14], the limited wafer area and high cost still makes general application not feasible. In 2015, H. Miyake et al. showed that face-to-face high temperature annealing (HTA) of AlN buffer layers can significantly improve the crystal quality by recrystallization [15,16]. The TDD reduction in AlN buffer layers is significant regardless of deposition method [17,18] and types of sapphire substrate [19–22]. After HTA technology showed its robustness and versatility for the AlN template, the demonstration of a more efficient UVC LED was expected. In 2020, C.Y. Huang et. al unraveled the difficulty in transferring the low TDD of an AlN buffer layer to the subsequent UVC LED layer stack and proposed a simple way to mitigate that [23]. In this report, we demonstrate that the optimal threading dislocation of the AlN buffer is around 7×10^8 cm^{-2} for a 1.6 μm thick $Al_{0.63}Ga_{0.37}N$ layer and discuss how we might lower this value for a more efficient UVC LED. The relevant defects of AlGaN growth on an

* Corresponding author.
E-mail address: cyhuang06@nycu.edu.tw (C.-Y. Huang).

https://doi.org/10.1016/j.jcrysgro.2022.126910
Received 7 August 2022; Received in revised form 16 September 2022; Accepted 27 September 2022
Available online 13 October 2022

ultra-low TDD AlN buffer are also explained with schematic and supporting materials characterizations such as atomic force image (AFM), transmission electron miscroscope (TEM) image, and cathodoluminescence (CL).

2. Experiment

2.1. MOVPE growth

The low-TDD AlN templates were grown by hydride vapor phase epitaxy (HVPE) by SCIOCS ltd., Japan. The thicknesses were all close to 300 nm and the initial full-width at half-maximum (FWHM) of X-ray rocking curves (XRC) on 102 reflection (102 FWHM, for brevity) ranged from 220 arcsec to 320 arcsec. AlN buffers with different 102 FWHMs were intentionally chosen for regrowth experiments. For convenience, these templates are called"HVPE-AlN" in the following paragraphs to differentiate them from AlN buffers grown by MOVPE at low temperature (LT-AlN).

The HVPE-AlN templates were used for AlGaN/AlN growth in a Taiyo-Nippon-Sanso SR-4000 MOVPE system. The growth temperature curve is schematically illustrated in Fig. 1. The temperature of AlN regrowth was 1220 ℃ with a growth rate of 0.9 μm/hr. If the targeted structure included *n*-AlGaN on top, the temperature was then ramped to 1060 ℃, and the growth rate of *n*-AlGaN was around 0.6 μm/hr. The precursors were ammonia, tri-methyl aluminum and tri-methyl gallium in H_2 carrier gas. Silane was injected for Si doping. The Si concentration in *n*-AlGaN and Si-doped AlN was 2.5×10^{19} cm^{-3} and 2.0×10^{19} cm^{-3}, respectively. Since the coefficient of thermal expansion (CTE, or α) of sapphire is larger than that of AlN, the AlN growth on LT-AlN will be tensilely strained, and the regrowth of AlN on HVPE-AlN which has seen higher temperatures becomes compressively strained instead [24,25].

2.2. Materials characterizations

The AlGaN/AlN crystal quality was assessed by a Malvern Panalytical X'Pert3 high-resolution X-ray diffractometer (HR-XRD) system. 002 ω-2θ rocking curves (XRC) reveal the lattice constant and strain state of HVPE-AlN and the regrown AlN. The TDD was evaluated from the 002/102 XRC FWHMs of the AlN or AlGaN diffraction peaks. The composition and strain state of AlGaN was assessed by 114 reciprocal space mapping (RSM) using the PIXcel3D array detector for fast measurement. The detailed extraction procedure of TDD, alloy composition, and strain state can be found in the supplement of reference 26. The surface was inspected by AFM. CL at low temperature (T = 10 K) was used to visualize the threading dislocations in *n*-AlGaN. A defective AlGaN sample was analyzed by crossectional TEM to observe the TDs in the epitaxy.

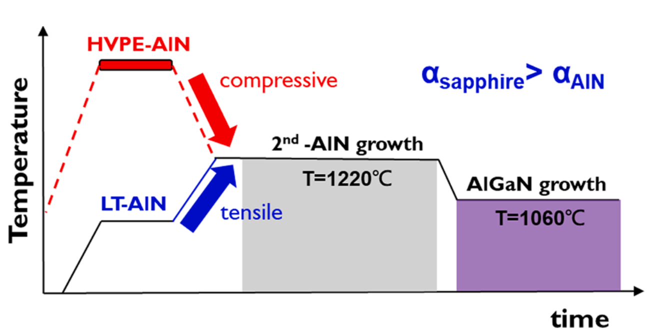

Fig. 1. Schematic growth temperature curve of AlGaN/AlN growth in MOVPE.

3. Result and discussion

3.1. Strain compensation by Si-doped AlN growth

The schematic structure of (a) 2.26 μm thick unintentionally-doped (UID) AlN layers grown on LT-AlN, (b) on HVPE-AlN, and (c) Si-doped AlN with varying thickness, h, from 2.17 μm to 2.98 μm grown on HVPE-AlN are shown in Fig. 2(a) to (c). 102 FWHMs of HVPE-AlN templates ranged from 272 arcsec to 315 arcsec. The in-plane strain states of the AlN layers are extracted from the peaks of 002 ω-2θ rocking curves (XRC) [26]. The UID AlN on either LT-AlN or HVPE-AlN shows a single peak, which implies that the strain state through the AlN layer is rather uniform. On the contrary, the Si-doped AlN on HVPE-AlN shows two peaks. The left peak with the smaller 2θ value is insensitive to the regrowth thickness, so it can be assigned to the HVPE-AlN template, while the right peak comes from the Si-doped AlN. The dependence of strain states on the regrowth AlN thickness are plotted in Fig. 2(d).

Note that all strain values are negative due to the cooling from growth temperature to room temperature (RT). AlN growth on LT-AlN buffer is known to be tensile at growth temperature [24,25]. The reference sample with LT-AlN (black square) was crack-free, indicating that it was only slightly tensile at growth temperature. The strain of HVPE-AlN at RT is more compressive and ranged from −0.26 % to −0.30 %. However, the strain of the Si-doped AlN top layer becomes

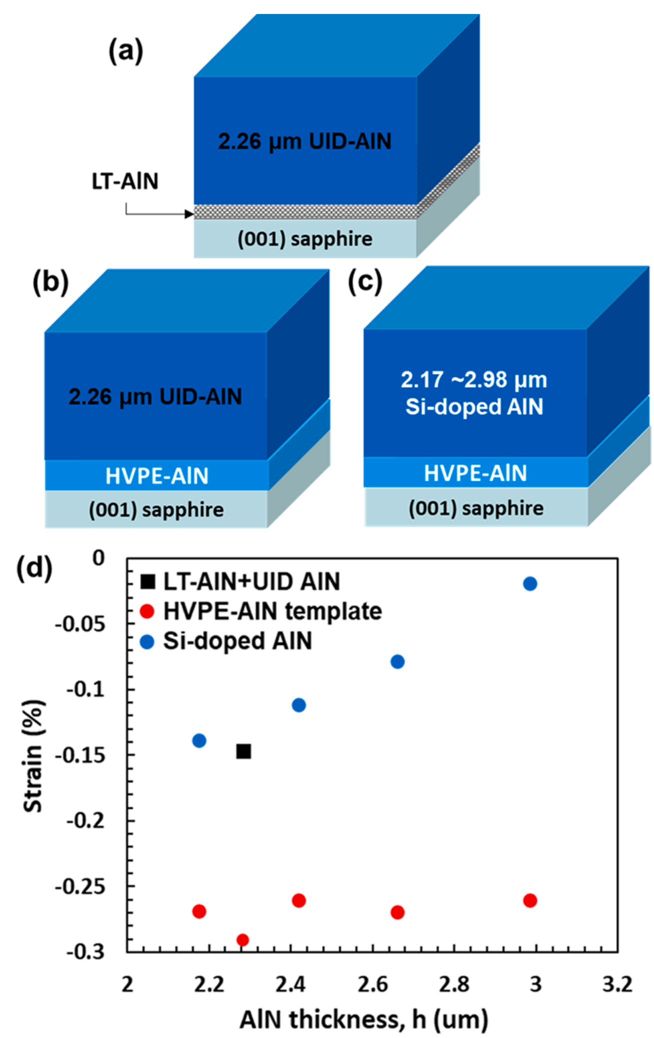

Fig. 2. The schematic strucutre of (a) 2.26 μm UID AlN on LT-AlN (b) 2.26 μm UID AlN on HVPE-AlN (c) 2.17–2.98 μm Si-doped AlN on HVPE-AlN (d) Extracted in-plane strains over AlN thicknesses.

more tensile than that of the reference sample for h > 2.2 μm. Therefore, further increasing the layer thickness bears the risk of cracking at growth temperature. The gradual strain evolution with thickness of Si-doped AlN is driven by surface-mediated dislocation tilt (SMDT) [27]. The schematic of SMDT proccess was illustrated in Fig. 3. SMDT occurs when III-vacancies on the growth surface interact with the core of threading edge dislocations. As a result, the crystal half-plane behind the edge dislocation shortens gradually as the film grows thicker. The effective in-plane lattice constant widens, and tensile strain is generated. The amount of tensile strain ($\Delta\varepsilon$) can be modeled by: [28].

$$\Delta\varepsilon = \frac{1}{2} b^{*} \rho_e{}^{*} tan\theta^{*} h \tag{1}$$

ρ_e is the the density of TDs with an edge component, b is the magnitude of the Burger's vector, and θ is the inclination angle of edge TDs. The vacancy concentration is high due to the self-compensation effect in Si-doped AlN, so SMDT is facilitated [29,30]. The compressive thermal strain from HVPE-AlN was therefore compensated by the tensile strain resulting from SMDT.

Eq. (1) indicates that $\Delta\varepsilon$ is proportional to the edge dislocation density, ρ_e. Therefore, strain compensation by SMDT will be inefficient if the ρ_e in AlN is very low. A thicker Si-doped AlN will be required to achieve the same amount of strain compensation. Fig. 4 plots the 2-inch wafer warpage over the ρ_e in the AlN layers. According to the Stoney's equation, the film stress is proportional to the curvature, and the curvature is proportional to the wafer warpage. Therefore, the wafer warpage is also an effective indicator to compare the strain state among samples if their overall thicknesses are similar. The reference sample with LT-AlN possessed a final ρ_e of 2.3×10^9 cm^{-2} and a warpage of 20 μm. The final ρ_e of AlN on HVPE-AlN was less than a quarter of the reference sample's ρ_e, but the warpage is upto 60 μm due to the higher compressive strain. We chose HVPE-AlN templates within a broad range of initial 102 FWHMs (220 arcsec to 280 arcsec) for MOVPE growth of Si-doped AlN. The warpage of the Si-doped AlN was lower than that of

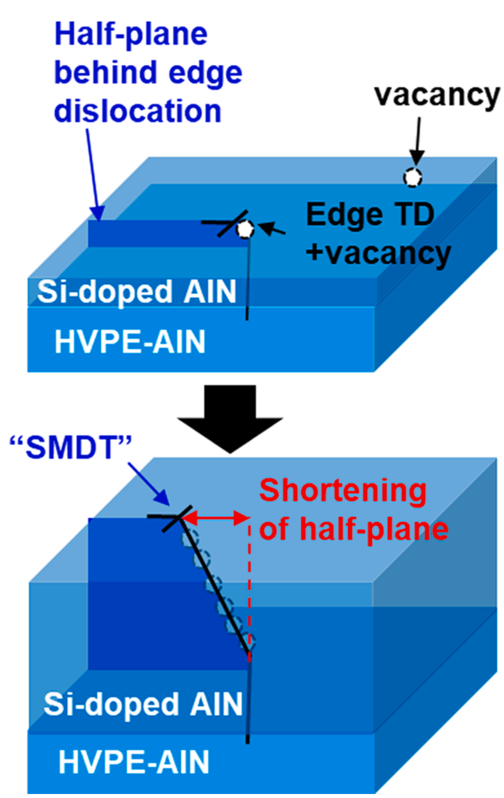

Fig. 3. The schematic of surfrace-mediated dislocation tilt (SMDT) in Si-doped AlN.

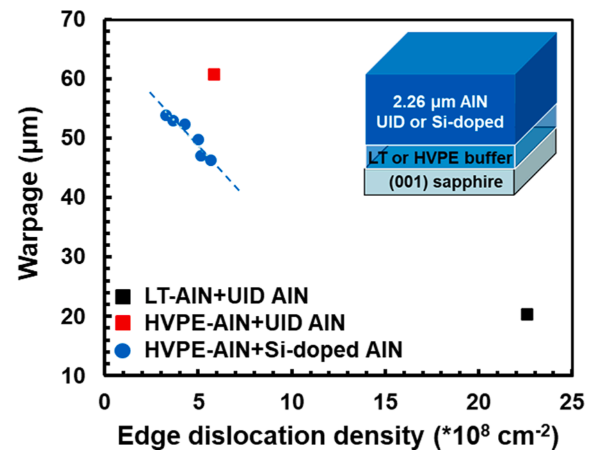

Fig. 4. Plot of the warpage of 2-inch wafers with 2.26 μm AlN on AlN buffer vs edge dislocation density in the top layer. The layer structure is schematically illustrated at the top-right corner.

the UD AlN layer due to strain compensation by SMDT and shows a strong negative correlation with the ρ_e (R^2 = 0.91). These results strongly suggest that the strain compensation by SMDT becomes ineffective if the edge dislocation density is too low.

3.2. Strain-induced phenomena in AlGaN growth

According to Vegard's Law, the mismatch strain of an $Al_{0.63}Ga_{0.37}N$ layer on freestanding AlN is −0.91 %. If the strain from the HVPE-AlN template is included, the strain of AlGaN on AlN could exceed −1.05 %. Therefore, if HVPE-AlN replaces the conventional LT-AlN buffer, strain-induced phenomena in AlGaN will be promoted. This includes: (a) TD tilt and misfit dislocation (MD) generation [31], (b) evolution of hump-like primary morphologies [32,33], (c) TD half-loop nucleation from the surface, and (d) evolution of plateau-like secondary morphologies. The schematic illustration and example AFM images are shown in Fig. 5. Although strain-induced TD half-loop nucleation has been observed in the InGaN/GaN system [34,35], the half-loop nucleation depicted in Fig. 5(c) was not confirmed in compressive AlN until 2022. [36] Fig. 5(d) is the AFM image of 2.0 μm $Al_{0.58}Ga_{0.42}N$ on 2.2 μm UID AlN on HVPE-AlN. Step flow was pinned by local defects and then terraces coalesced into macroscopic step bunches with tens of nanometers height. Although the plateau-like morphology is related to the film's compressive strain, the formation mechanism requires more detailed investigation. Nevertheless, after the secondary morphology with step bunches appears, fabrication of a functional LED device is no more probable. On the other hand, the phenomena of Fig. 5(a) and (b) are not neccessarily detrimental to crystal quality. If there is no interaction between the tilted or glided dislocations, the TDD remains invariant after strain relaxation; if a pair of tilted/glided TDs with opposite signs meet, the TDD is lowered due to mutual annihilation. As a result, a micrometer-thick AlGaN layer could be grown without drastically increasing the TDD or surface roughness. In other words, the AlGaN epitaxial growth is stabilized by strain relaxation via pre-existing TDs. However, if the amount of pre-existing TD is too low, TD half-loop nucleation from the surface becomes the prevailing relaxation mechanism. As a result, the TDD increases and the crystal quality of subsequent device layers deteriorates. For example, Fig. 5(e) is a cross-sectional TEM image of 1.6 μm $Al_{0.63}Ga_{0.37}N$ on 3.4 μm Si-doped AlN and HVPE-AlN. The TDD of HVPE-AlN was estimated to be 4.5×10^8 cm^{-2} by HR-XRD. Although SMDT in Si-doped AlN occured, many nearly-horizonal lines defects emerged in the AlGaN layer. We inferred those horizontal lines to be segment of TD half-loop injected from the growth surface as depicted in Fig. 5(c).

To suppress the TD nucleation, an intuitive approach is to reduce the

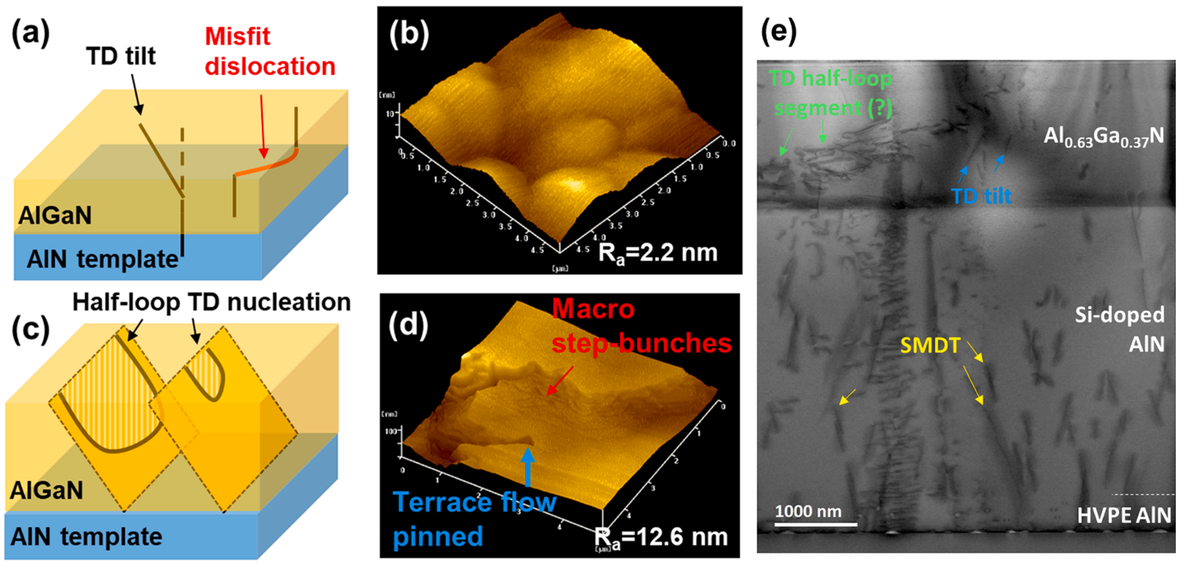

Fig. 5. Schematic illustration of AlGaN strain relaxation via (a) TD tilt and MD generation and (c)TD half-loop nucleation from surface. 5 μm × 5 μm AFM images of (b) primary and (d) secondary morphologies of compressive AlGaN epitaxy. (e) cross-sectional TEM image of a 1.6 μm $Al_{0.63}Ga_{0.37}N$ and 3.4 μm Si-doped AlN on HVPE-AlN with a very low initial TDD.

thickness or Ga content of AlGaN layers in an UVC LED heterostructure. However, both a reduced thickness or a wider bandgap of current injection/spreading layers compromise the LED's electrical characteristics. A thinner current spreading layer yields a higher sheet resistance, and a higher bandgap results in decreased donor activation and usually higher contact resistance. Both effects yield a higher forward voltage and a compromised wall-plug efficiency (WPE). The more constructive approach is to compensate the strain of the AlN template by SMDT. On AlN templates with a widened in-plane lattice, the initial mismatch strain of the same AlGaN is lowered, so the strain-induced TD nucleation will be postponed. As a result, the design window of *n*-AlGaN composition and thickness is broadened. For example, Fig. 6 shows the CL images of the same *n*-AlGaN grown on similar low-TDD HVPE-AlN templates. The regrown AlN is UID and Si-doped in Fig. 6(a) and (b), respectively. Only Fig. 6(a) reveals a high TDD. Therefore, we can infer that a 1.6 μm n-$Al_{0.63}Ga_{0.37}N$ layer requires prior strain compensation by Si-doping and resulting SMDT in the regrown AlN on HVPE-AlN template in order to achieve a low TDD for further growth.

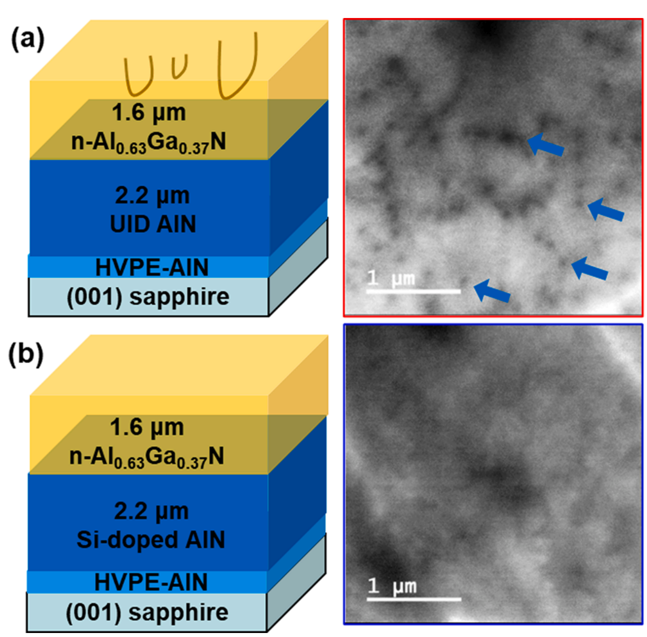

Fig. 6. The schematic structure and 3.5 μm × 3.5 μm panchromatic CL images of $Al_{0.63}Ga_{0.37}N$ on (a) UID AlN and (b) Si-doped AlN on HVPE-AlN template. The blue arrows in (a) mark some additional dark spots due to TD nucleation. (For interpretation of the references to colour in this figure legend, the reader is referred to the web version of this article.)

3.3. *The optimal dislocation density of the AlN buffer*

In summary, if the TDD of the AlN buffer is high, the TDD in *n*-AlGaN is naturally high due to TD propagation and will decrease with AlGaN thickness by dislocation annihilation at the cost of increased wafer bow. However, if the TDD of the buffer is very low, strain compensation by SMDT become ineffective, and the resulting TDD in the active region increases due to TD half-loop nucleation and resulting TD segments. Therefore, for a given *n*-AlGaN spreading layer in an UVC LED, an optimal range of TDD of the AlN buffer exists. Fig. 7 plots the edge TDDs of the same *n*-AlGaN on Si-doped AlN buffer over the TDD of the employed HVPE-AlN templates. The TDDs of single Si-doped AlN layer

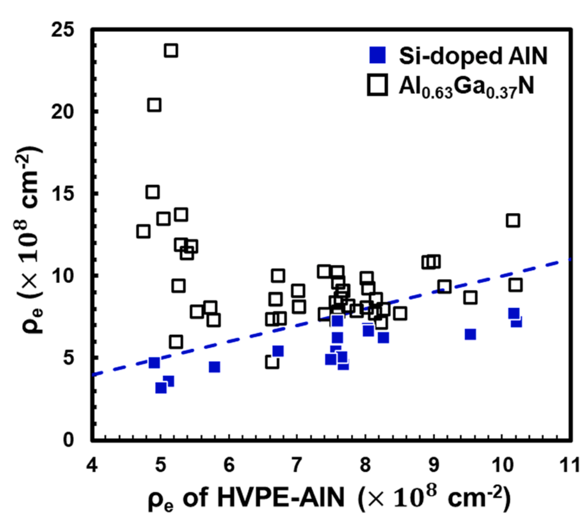

Fig. 7. The dependence of edge TDD of *n*-AlGaN and Si-doped AlN on its initial edge TDD of HVPE-template.

in Fig. 2 are also included. The TDD in the Si-doped AlN is proportional to that in the HVPE-AlN template (blue dashed line). The TDD of *n*-AlGaN on Si-doped AlN becomes unstable and could drastically increases when the TDD of the template is less than 6×10^8 cm^{-2}. Therefore, we conclude that the optimal dislocation density in the AlN template is around 7×10^8 cm^{-2}, where the low TDD from the Si-doped AlN buffer can be still maintained to the above device *epi* with a decent reproducibility.

To lower the optimal TDD in UVC LED epitaxy, the straightforward approach is still to reduce the thickness and Ga content of the *n*-AlGaN current spreading/contact layer to delay TD nucleation. Whether the accompanying cost is worthwhile requires further validation with device results. Inserting more tensile strain in the underlying layer might be effective. However, as mentioned in section 3.1, the required Si-doped AlN thickness will be high, and the extent of compensation will be limited by the risk of crack formation in the AlN buffer. One might also consider constructing a metamorphic AlGaN multilayer or re-optimize the growth conditions to delay the TD nucleation. In general, UVC LEDs with a shorter emitting wavelength shall possess a lower limit for the optimal TDD of the buffer since less Ga is required for the electron injection and spreading layer resulting in lower misfit strain.

4. Conclusions

In conclusion, we revealed the limits and possibilities of low-TDD AlN templates for UVC LED. The inherent thermal strain in the templates can be compensated by SMDT when using Si-doped AlN buffer layers, but the effectiveness of compensation is limited by a low TDD in the buffer as well. The small number of pre-existing dislocations available for strain relaxation triggers TD nucleation from the surface, which is detrimental to the crystal quality of subsequent device layers. As a result, an optimal range of TDD exists for a specific AlGaN/AlN bilayer structure on low-TDD AlN templates. Therefore, the utilization of low-TDD AlN templates requires careful adjustment of the layer design as well as the growth parameters to further improve the IQE and WPE of full UVC LED structure simultaneously.

CRediT authorship contribution statement

Chia-Yen Huang: Conceptualization, Methodology, Writing – original draft. **Sylvia Hagedorn:** Investigation, Validation. **Sebastian Walde:** Investigation. **Chia-Lung Tsai:** Resources. **Yi-Keng Fu:** Supervision, Project administration. **Markus Weyers:** Supervision, Writing – review & editing.

Declaration of Competing Interest

The authors declare that they have no known competing financial interests or personal relationships that could have appeared to influence the work reported in this paper.

Data availability

The authors do not have permission to share data.

Acknowledgement

This study is partly funded by the Ministry of Science and Technology of Taiwan under the project contact number MOST 111-2628-E-A49-023-.

References

[1] Q. Dai, M.F. Schubert, M.H. Kim, J.K. Kim, E.F. Schubert, D.D. Koleske, M. H. Crawford, S.R. Lee, A.J. Fischer, G. Thaler, M.A. Banas, Appl. Phys. Lett. 94 (2009) 111109.
[2] T. Nakano, Y. Harashima, K. Chokawa, K. Shiraishi, A. Oshiyama, Y. Kangawa, S. Usami, N. Mayama, K. Toda, A. Tanaka, Y. Honda, H. Amano, Appl. Phys. Lett. 117 (2020) 012105.
[3] S.F. Chichibu, A. Uedono, T. Onuma, B.A. Haskell, A. Chakraborty, T. Koyama, P. T. Fini, S. Keller, S.P. DenBaars, J.S. Speck, U.K. Mishra, S. Nakamura, S. Yamaguchi, S. Kamiyama, H. Amano, I. Akasaki, J. Han, T. Sota, Nat. Mater. 5 (2006) 810.
[4] M.K. Horton, S. Rhode, S.-L. Sahonta, M.J. Kappers, S.J. Haigh, T.J. Pennycook, C. J. Humphreys, R.O. Dusane, M.A. Moram, Nano Lett. 15 (2015) 923.
[5] H. Amano, N. Sawaki, I. Akasaki, Appl. Phys. Lett. 48 (1986) 353.
[6] S. Nakamura, Jpn. J. Appl. Phys. 30 (1991) L1705.
[7] H.-Y. Shin, S.K. Kwon, Y.I. Chang, M.J. Cho, K.H. Park, J. Crystal Growth 311 (2009) 4167.
[8] M.J. Cicha, R.I. Aldaz, A. Chakraborty, A. David, M.J. Grundmann, A. Tyagi, M. Zhang, F.M. Steranka, M.R. Krames, Appl. Phys. Lett. 101 (2012) 223509.
[9] R.G. Banal, M. Funato, Y. Kawakami, Phys. Status Solidi B 7 (2010) 2111.
[10] H. Kröncke, S. Figge, T. Aschenbrenner, D. Hommel, J. Cryst. Growth 381 (2013) 100.
[11] P. Caban, M. Rudzinski, M. Wojcik, J. Gaca, W. Strupinski, J. Cryst. Growth 414 (2015) 81.
[12] V. Kueller, A. Knauer, F. Brunner, U. Zeimer, H. Rodriguez, M. Kneissl, M. Weyers, J. Cryst. Growth 315 (2011) 200.
[13] M. Conroy, V.Z. Zubialevich, H. Li, N. Petkov, J.D. Holmes, P.J. Parbrook, J. Mater. Chem. C 3 (2015) 431.
[14] Y. Kumagai, Y. Kubota, T. Nagashima, T. Kinoshita, R. Dalmau, R. Schlesser, B. Moody, J. Xie, H. Murakami, A. Koukitu, Z. Sitar, Appl. Phys. Exp. 5 (2012) 055504.
[15] H. Miyake, C.H. Lin, K. Tokoro, K. Hiramatsu, J. Crystal Growth 456 (2016) 155.
[16] S. Xiao, R. Suzuki, H. Miyake, S. Harada, T. Ujihara, J. Crystal Growth 502 (2018) 44.
[17] C.Y. Huang, P.Y. Wu, K.S. Chang, Y.-H. Lin, W.C. Peng, Y.Y. Chang, J.P. Li, H. W. Yen, Y.C. Sermon Wu, H. Miyake, H.C. Kuo, AIP Adv. 7 (2017) 055110.
[18] H. Fujikura, T. Konno, T. Kimura, H. Miyake, Appl. Phys. Exp. 13 (2020) 025506.
[19] C.H. Lin, Y. Yamashita, H. Miyake, K. Hiramatsu, J. Crystal Growth 468 (2017) 845.
[20] S. Xiao, N. Jiang, K. Shojiki, K. Uesugi, H. Miyake, Jpn. J. Appl. Phys. 58 (2019) SC1003.
[21] M. Jo, Y. Itokazu, S. Kuwaba, H. Hirayama, J. Crystal Growth 507 (2019) 307.
[22] S. Hagedorn, S. Walde, A. Knauer, N. Susilo, D. Pacak, L. Cancellara, C. Netzel, A. Mogilatenko, C. Hartmann, T. Wernicke, M. Kneissl, M. Weyers, Phys. Stat. Sol. A 217 (2020) 1901022.
[23] C.Y. Huang, S. Walde, C.L. Tsai, C. Netzel, H.H. Liu, S. Hagedorn, Y.R. Wu, Y.K. Fu, M. Weyers, Jpn. J. Appl. Phys. 59 (2020) 070904.
[24] F. Brunner, V. Hoffmann, A. Knauer, E. Steimetz, T. Schenk, J.-T. Zettler, M. Weyers, J. Crystal Growth 298 (2007) 202.
[25] S. Walde, S. Hagedorn, M. Weyers, Jpn. J. Appl. Phys. 58 (2019) SC1002.
[26] S. Walde, C.Y. Huang, C.L. Tsai, W.H. Hsieh, Y.K. Fu, S. Hagedorn, H.W. Yen, T. C. Lu, M. Weyers, C.Y. Huang, Acta Mater. 226 (2022) 117625.
[27] D.M. Follstaedt, S.R. Lee, A.A. Allerman, J.A. Floro, J. Appl. Phys. 105 (2009) 083507.
[28] E. Romanov, J.S. Speck, Appl. Phys. Lett. 83 (2003) 2569.
[29] J.S. Harris, J.N. Baker, B.E. Gaddy, I. Bryan, Z. Bryan, K.J. Mirrielees, P. Reddy, R. Collazo, Z. Sitar, D.L. Irving, Appl. Phys. Lett. 112 (2018) 152101.
[30] A. Mogilatenko, A. Knauer, U. Zeimer, C. Hartmann, H. Oppermann, M. Weyers, J. Crystal Growth 462 (2017) 18.
[31] Z. Wu, K. Nonaka, Y. Kawai, T. Asai, F.A. Ponce, C. Chen, M. Iwaya, S. Kamiyama, H. Amano, I. Akasaki, Appl. Phys. Exp. 3 (2010) 111003.
[32] C.Y. Huang, K.S. Chang, C.Y. Huang, Y.H. Lin, W.C. Peng, H.W. Yen, R.M. Lin, H. C. Kuo, Appl. Phys. Lett. 111 (2017) 072110.
[33] Demir, Y. Koçak, A.E. Kasapoğlu, M. Razeghi, E. Gür, S. Elagoz, Semicond. Sci. Technol. 34 (2019) 075028.
[34] R. Liu, J. Mei, S. Srinivasan, F.A. Ponce, Appl. Phys. Lett. 89 (2006) 201911.
[35] A.V. Lobanova, A.L. Kolesnikova, A.E. Romanov, S.Y. Karpov, M.E. Rudinsky, E. V. Yakovlev, Appl. Phys. Lett. 103 (2013) 152106.
[36] A. Mogilatenko, S. Walde, S. Hagedorn, C. Netzel, C.Y. Huang, M. Weyers, J. Appl. Phys. 131 (2022) 045702.